Marine boundary layer clouds at the heart of tropical cloud feedback uncertainties in climate models

Sandrine Bony and Jean-Louis Dufresne

Laboratoire de Météorologie Dynamique, IPSL, Paris, France

The radiative response of tropical clouds to global warming exhibits a large spread among climate models, and this constitutes a major source of uncertainty for climate sensitivity estimates. To better interpret the origin of that uncertainty, we analyze the sensitivity of the tropical cloud radiative forcing to a change in sea surface temperature that is simulated by 15 coupled models simulating climate change and current interannual variability. We show that it is in regimes of large-scale subsidence that the model results (1) differ the most in climate change and (2) disagree the most with observations in the current climate (most models underestimate the interannual sensitivity of clouds albedo to a change in temperature). This suggests that the simulation of the sensitivity of marine boundary layer clouds to changing environmental conditions constitutes, currently, the main source of uncertainty in tropical cloud feedbacks simulated by general circulation models. **Citation:** Bony, S., and J.-L. Dufresne (2005), Marine boundary layer clouds at the heart of tropical cloud feedback uncertainties in climate models, *Geophys. Res. Lett.*, 32, L20806, doi:10.1029/2005GL023851.

1. Introduction

For more than a decade, the large spread of cloud feedbacks among climate models has been considered a major source of uncertainty for climate sensitivity estimates (*Cess et al.* [1990]; *Houghton et al.* [2001]; *Colman* [2003]; *Stephens* [2005]). The representation of convective and boundary-layer processes, in addition to the parameterization of cloud properties, is known to be critical for the prediction of the clouds response to climate change (e.g. *Senior and Mitchell* [1993]; *Yao and Genio* [1999]), and it differs widely among models. Whether the spread of cloud feedbacks among current models results primarily from different responses of deep convective clouds, boundary-layer clouds or both remains an open question.

To investigate this issue, we examine the radiative response of clouds to a change in environmental conditions which is predicted over tropical oceans (30^{o}S-30^{o}N) by 15 coupled ocean-atmosphere general circulation models (OAGCMs) that have performed simulations in support of the Fourth Assessment Report of the Intergovernmental Panel on Climate Change. First, we consider idealized climate change scenarios in which the atmospheric concentration of carbon dioxide increases by 1% per year, and we analyze the large-scale conditions in which the tropical clouds response to global warming is the most different among models. Second, we analyze observations and 20th century simulations performed by the same models to explore how the radiative effect of clouds (referred to as the cloud radiative forcing or CRF) is affected by a change in environmental conditions at the interannual timescale, and to investigate in what situations the disagreement is the greatest among models, and between models and observations.

2. Compositing by dynamical regimes

In the tropics, the relative occurrence of the different cloud types strongly depends on the large-scale atmospheric circulation. By using the monthly-mean mid-tropospheric (500 hPa) vertical pressure velocity ω as a proxy for large-scale rising ($\omega < 0$) or sinking ($\omega > 0$) motions, we decompose the large-scale tropical circulation as a series of dynamical regimes defined from ω (bins of 5 hPa/d), and we compute composites of climate variables in these regimes (*Bony et al.* [2004]). To a first approximation, this methodology allows us to segregate regimes of deep convection and upper-level cloud tops from regimes of shallow convection and low-level cloud tops (Figure 1). The frequency distribution P_ω of the different dynamical regimes shows that situations of large-scale subsidence are by far the most frequent over tropical oceans. These situations primarily occur over the trade winds and at the eastern side of the ocean basins (not shown). Marine boundary layer (MBL) clouds, topped by the low-level trade inversion, constitute the most prevalent cloudiness in these regimes (*Norris* [1998b], *Wyant et al.* [2005]).

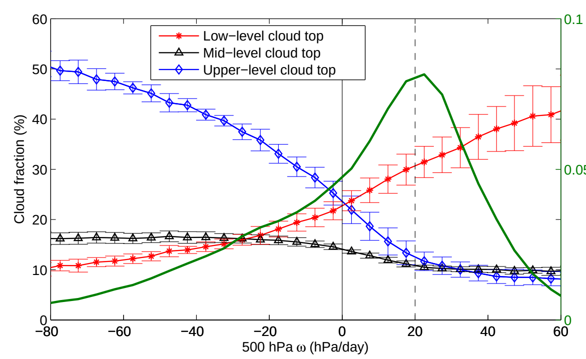

Figure 1. Satellite-derived fractional area covered by low-level, mid-level and upper-level clouds (as classified by the International Satellite Cloud Climatology Project ISCCP, *Rossow and Schiffer* [1999]) binned by ERA40 monthly-mean mid-tropospheric vertical velocity ω over tropical oceans for 1984-2000. Also reported (thick solid line) is the mean probability distribution function (P_ω) of the different dynamical regimes (bins of ω of 5 hPa/d). The cumulated frequency of occurrence of all regimes $\omega > 20 hPa/d$ is about 30%.

Since the dynamics is partly tied to the SST distribution, regional changes in CRF may be related to changes in both

0094-8276/05/2005GL023851$5.00

the large-scale flow and local thermodynamic conditions. To better isolate the influence on CRF of a change in surface or boundary-layer conditions, we examine the temporal covariation of CRF and SST anomalies under specified dynamical conditions.

3. Analysis of the CRF response to SST under climate change

From 1% per year CO_2 increase simulations of each OAGCM, we estimate the long-term climate change response of the CRF to SST by computing 80-year time series (up to CO_2 doubling) of CRF and SST composites in dynamical regimes (these composites are referred to as C_ω and T_ω). In each regime, we compute monthly interannual anomalies (δC_ω and δT_ω) by substracting the mean seasonal cycle of C_ω and T_ω calculated over the first 10 years of the simulation. Then we fit the long-term evolution of δC_ω and δT_ω through a simple linear trend over time to extract the long-term response of clouds and temperature to forced climate change (long-term, linear evolutions are referred to as $\delta\tilde{C}_\omega$ and $\delta\tilde{T}_\omega$, respectively) from shorter-term variability. Finally, in each dynamical regime the CRF sensitivity to SST associated with climate change is calculated as the linear regression coefficient: $S_\omega^{CO2} = \partial\delta\tilde{C}_\omega / \partial\delta\tilde{T}_\omega$. For each model, the tropical-mean climate change response of CRF to surface warming is given by: $\Sigma = \int_{-\infty}^{+\infty} P_\omega S_\omega^{CO2} d\omega$.

Model estimates of Σ exhibit a large spread, ranging from -2.0 to +1.6 $Wm^{-2}K^{-1}$ with a standard deviation of 1 $Wm^{-2}K^{-1}$. This spread is mostly controlled by the SW component of Σ (standard deviations of Σ^{SW} and Σ^{LW} equal 1.1 $Wm^{-2}K^{-1}$ and 0.4 $Wm^{-2}K^{-1}$, respectively). We note a positive correlation (0.80) between Σ and the warming of tropical oceans at the time of CO_2 doubling: models that simulate a less negative CRF and thus a reduced cooling effect of tropical clouds in response to global change ($\Sigma > 0$) predict, on average, a higher tropical warming (ΔT = 1.7 K $\pm$ 0.3 K) than models that simulate an enhanced cooling effect of tropical clouds ($\Sigma < 0$, ΔT = 1.2 K $\pm$ 0.2 K). The radiative response of clouds to surface warming seems thus critical to the magnitude of tropical climate change projections. Hereafter, we will refer to the 7 models that predict $\Sigma < 0$ and to the 8 models that predict $\Sigma > 0$ as low-sensitivity (LS) and high-sensitivity (HS) models, respectively.

To interpret the range of Σ estimates, we compare the CRF response to SST changes that is predicted in each dynamical regime by the two groups of models (S_ω^{CO2}, Figure 2). While the LW CRF response is weak and roughly similar among the models, LS models predict for $\omega > 0$ a much weaker SW CRF response than HS models. This constrast is further amplified by the large statistical weight (P_ω) of subsidence regimes. Therefore, most of the spread of Σ estimates arises from model differences in the SW response of clouds to temperature in regimes of shallow convection. In comparison, differences of CRF sensitivity in deep convective regimes constitute a much weaker source of spread.

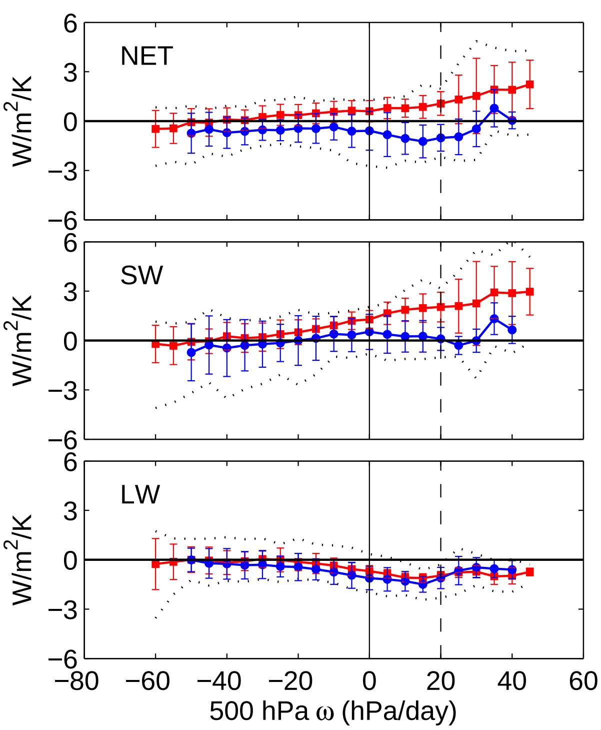

Figure 2. Sensitivity of the NET, SW and LW CRF to SST changes within dynamical regimes derived from idealized climate change scenarios (S_ω^{CO2}). Dotted lines show the minimum and maximum values of S_ω^{CO2} predicted by the 15 OAGCMs. Lines with red squares (blue circles) show the mean and the standard deviation of the sensitivity of the 8 HS models predicting $\Sigma > 0$ (7 LS models predicting $\Sigma < 0$, respectively).

4. Interannual sensitivity of the CRF to SST

Given the diversity of CRF responses predicted by models under climate change, it is crucial to evaluate the change in clouds that is simulated by climate models in response to a change in environmental conditions. Many observational tests should be considered for that purpose. Here, we consider the change in CRF that occurs at the interannual timescale in response to a change in SST. Note that this change is considered as an *example* of response to a change in environmental conditions (temperature, static stability, relative humidity, etc), not as an *an analogue* of the CRF response to long-term, global climate changes.

The interannual CRF sensitivity to SST (S_ω^{20C}) is estimated from observations or from simulations through a procedure similar to that described above, except that the mean seasonal cycle is defined over the period 1985-89, and that S_ω^{20C} is defined as $\partial\delta C_\omega / \partial\delta T_\omega$. Observational estimates are derived from 17-year time series (1984-2000) of 2.5^o x 2.5^o monthly-mean data of SST (*Reynolds et al.* [2002]) and of ISCCP-FD radiative fluxes[1] (*Zhang et al.* [2004]), and large-scale estimates of ω derived from global reanalyses. Estimates of S_ω^{20C} are computed using ω from either the 40 year re-analysis ERA40[2] or the NCEP-DOE AMIP-II Reanalysis (*Kanamitsu et al.* [2002]), and 5%-95% confidence intervals are computed for each estimate. We define the range of observational estimates of S_ω^{20C} as the envelope of both confidence intervals[3].

The interannual sensitivity of the NET CRF to SST inferred from observations is positive in all dynamical regimes and ranges from 0 to 6 $Wm^{-2}K^{-1}$ (Figure 3). In convective regimes, both the LW and SW components of S_ω^{20C} contribute to that result, while in regimes primarily associated with MBL clouds ($\omega > 20$ hPa/d), this is associated with a negligible change in LW CRF and a large reduction of the SW CRF (and thus a positive anomaly) as SST rises. Several observational studies have already pointed out the decrease of low-clouds optical thickness and albedo with increasing temperature in tropical subsidence areas (*Tselioudis et al.* [1992]; *Greenwald et al.* [1995]; *Bony et al.* [1997]). By using longer time series and by examining the CRF dependence on SST for given dynamical conditions, we find here that the weakening of SW CRF with rising SST ($S_\omega^{20C,SW} > 0$) occurs in all regimes of the tropical circulation, and that it is *maximum* in regions of strong subsidence. The reasons for that large sensitivity might be related to the breakup, as SST increases, of stratiform low-level cloud types (stratus, stratocumulus) into more cumuliform clouds (trade cumulus), and thus to a smaller cloud fraction and a less negative SW CRF. Such a transition can occur if the SST increase is associated with a decrease of the lower tropospheric static stability and/or with an increase of the planetary boundary-layer (PBL) decoupling (*Klein and Hartmann* [1993]; *Pincus et al.* [1997]; *Norris* [1998a]; *Wood and Bretherton* [2004]). The thinning of cloud layers with increasing temperature (*Del Genio and Wolf* [2000]), as well as the increase in precipitation efficiency of light rain (*Lau and Wu* [2003]) might also contribute to decrease the clouds optical depth and weaken the SW CRF as SST increases.

Despite a wide envelope of model estimates[4], over most dynamical regimes the majority of OAGCMs predict CRF sensitivities to interannual SST changes in agreement with the range of observational estimates, and little difference is found on average between LS and HS models (Figure 3). However, an important exception occurs for ω larger than about 30 hPa/d, where almost 90% of the models (13 out of 15) underestimate the SW and NET components of S_ω^{20C}. It is also in these regimes that the interannual CRF sensitivities of LS and HS models are the most different, with LS models underestimating slightly more the CRF sensitivity than HS models.

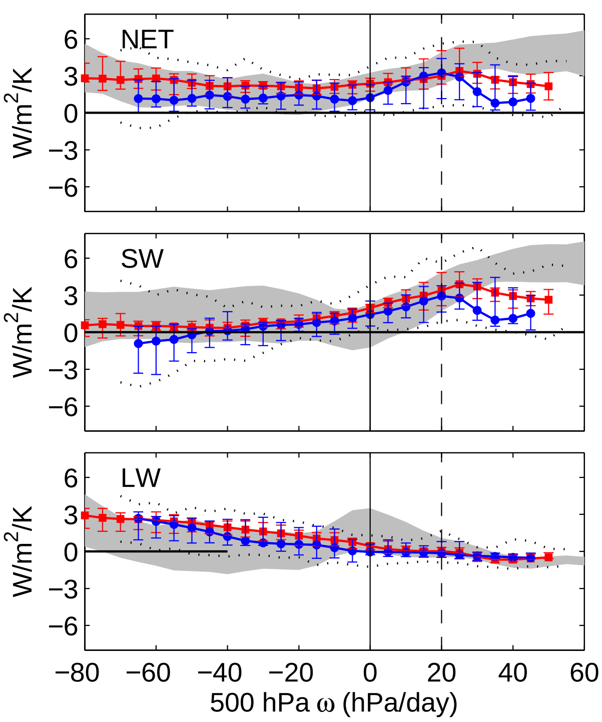

Figure 3. Sensitivity of the NET, SW and LW CRF to SST changes within dynamical regimes derived from observations and from 20th century simulations (S_ω^{20C}). The shaded area shows the 5%-95% confidence interval of observational estimates derived from satellite data and reanalyses. Dotted lines show the minimum and maximum values of S_ω^{20C} predicted by the 15 OAGCMs. Lines with red squares show the median, 25th and 75th percentiles of the sensitivity predicted by the 8 HS models that predict $\Sigma > 0$ in climate change. Lines with blue circles show the same for the 7 LS models that predict $\Sigma < 0$ in climate change.

5. Conclusion and discussion

In the tropics, it is in regimes of large-scale subsidence, where MBL clouds prevail, that the radiative response of clouds to a change in surface temperature (1) differs most in climate change among models and (2) disagrees most with observations in the current climate. This combination suggests that, currently, MBL clouds are at the heart of tropical cloud feedback uncertainties in climate models.

Most models underestimate the interannual sensitivity of MBL clouds albedo to a change in temperature, with HS models performing better than LS models *on average* (there is some variability among models of the same group). The difficulty that OAGCMs have in reproducing the observed large CRF sensitivity to SST in subsidence regimes suggests that some underlying physical processes are missing or poorly represented in the models. This presumably reveals problems in the representation of planetary boundary-layer processes and MBL clouds, and more specifically in the *sensitivity* of MBL clouds to changing surface and PBL properties.

Since widespread changes in surface and PBL properties are expected under climate change, the weakness and the diversity of models performance in simulating the sensitivity of MBL clouds to changing environmental conditions are likely to translate into diversity and uncertainty in the response of MBL clouds to global warming. It presumably explains part of the spread of tropical cloud feedbacks discussed in section 3. It may contribute also to the inability of climate models to simulate decadal variations of the Earth's radiation budget as large as those observed (*Wielicki et al.* [2002]).

As stressed by other studies (*Webb et al.* [2001]; *Volodin* [2004]), it is thus crucial to improve the representation of MBL clouds in climate models. However, we insist that it is the *sensitivity* of clouds to changing environmental conditions that needs to be assessed. For that purpose, considering only the CRF sensitivity is not sufficient because radiative sensitivities consistent with observations may be obtained through compensating errors in the sensitivity of cloud geometrical and optical properties. Moreover, it will be important to understand the physical processes that govern the clouds response to climate change, and to determine whether some of these processes are involved also in the clouds response to interannual variations. For instance, if the reduction of the SW CRF with increasing temperature predicted by a model in climate change corresponds to a stratocumulus to cumulus transition, then assessing the ability of this model to reproduce such transitions in the current climate might constitute a constraining test for climate sensitivity. More generally, process studies leading to a better assessment of the behaviour of MBL clouds with changing environmental conditions will have the potential to reduce substantially the uncertainty in model predictions of tropical cloud feedbacks and climate sensitivity.

Acknowledgments. We acknowledge the international modeling groups for providing their data for analysis, the PCMDI for collecting and archiving the model data, the JSC/CLIVAR WGCM and their Coupled Model Intercomparison Project (CMIP) and Climate Simulation Panel for organizing the model data analysis activity, and the IPCC WG1 TSU for technical support. The IPCC Data Archive at LNNL is supported by the Office of Science, U.S. Department of Energy. We thank W. Rossow, G. Sèze and M. Viollier for useful discussions, and two anonymous reviewers for helpful comments and suggestions.

Notes

1. As shown in the supporting material, interannual anomalies of the CRF derived from ISCCP-FD fluxes are in very good agreement with those derived from the Earth Radiation Budget Experiment over the period 1985-89.
2. Documentation of the European Centre for Medium-Range Weather Forecasts (ECMWF) 40 year re-analysis (ERA40) is available at http://www.ecmwf.int/products/data/archive/descriptions/e4/
3. More information is included in the supporting material available via Web browser or via Anonymous FTP from ftp://ftp.agu.org/apend/" (Username = "anonymous", Password = "guest").
4. Interannual sensitivities derived from individual OAGCMs are shown in the supporting material.

References

Bony, S., K.-M. Lau, and Y. C. Sud (1997), Sea surface temperature and large-scale circulation influences on tropical greenhouse effect and cloud radiative forcing, *J. Climate*, *10*, 2055–2077.

Bony, S., J.-L. Dufresne, H. LeTreut, J.-J. Morcrette, and C. Senior (2004), On dynamic and thermodynamic components of cloud changes, *Climate Dyn.*, *22*, 71–86.

Cess, R., et al. (1990), Intercomparison and interpretation of cloud-climate feedback processes in nineteen atmospheric general circulation models, *J. Geophys. Res.*, *95*, 16,601–16,615.

Colman, R. (2003), A comparison of climate feedbacks in general circulation models, *Climate Dyn.*, *20*, 865–873.

Del Genio, A. D., and A. B. Wolf (2000), The temperature dependence of the liquid water path of low clouds in the southern great plains, *J. Climate*, *13*, 3465–3486.

Greenwald, T. J., G. L. Stephens, S. A. Christopher, and T. H. V. Haar (1995), Observations of the global characteristics and regional radiative effects of marine cloud liquid water, *J. Climate*, *8*, 2928–2946.

Houghton, J. T., Y. Ding, D. J. Griggs, M. Noguer, P. J. van der Linden, X. Dai, K. Maskell, and C. A. Johnson (2001), *Climate Change 2001: The Scientific Basis.*, 49 pp., Cambridge Univ. Press, Cambridge.

Kanamitsu, M., W. Ebisuzaki, J. Woollen, S.-K. Yang, J. Hnilo, M. Fiorino, and G. L. Potter (2002), NCEP-DOE AMIP-II Reanalysis (R-2)., *Bull. Amer. Meteor. Soc.*, *83*, 1631–1643.

Klein, S. A., and D. L. Hartmann (1993), The seasonal cycle of low stratiform clouds., *J. Climate*, *6*, 1587–1606.

Lau, K.-M., and H. T. Wu (2003), Warm rain processes over tropical oceans and climate implications, *Geophys. Res. Lett.*, *30*, doi:10.1029/2003GL018,567.

Norris, J. R. (1998a), Low cloud type over the ocean from surface observations. Part I: relationship to surface meteorology and the vertical distribution of temperature and moisture., *J. Climate*, *11*, 369–382.

Norris, J. R. (1998b), Low cloud type over the ocean from surface observations. Part II: geographical and seasonal variations., *J. Climate*, *11*, 383–403.

Pincus, R., M. B. Baker, and C. S. Bretherton (1997), What controls stratocumulus radiative properties ? lagrangian observations of cloud evolution., *J. Atmos. Sci.*, *54*, 2215–2236.

Reynolds, R. W., N. A. Rayner, T. M. Smith, and D. C. Stokes (2002), An improved in situ and satellite sst analysis for climate., *J. Climate*, *15*, 1609–1625.

Rossow, W. B., and R. A. Schiffer (1999), Advances in understanding clouds from ISCCP, *Bull. Amer. Meteor. Soc.*, *80*, 2261 2287.

Senior, C. A., and J. F. B. Mitchell (1993), Carbon dioxide and climate. The impact of cloud parameterization, *J. Climate*, *6*, 393–418.

Stephens, G. L. (2005), Cloud feedbacks in the climate system: a critical review, *J. Climate*, *18*, 237–273.

Tselioudis, G., W. B. Rossow, and D. Rind (1992), Global patterns of cloud optical thickness variation with temperature, *J. Climate*, *5*, 1484–1495.

Volodin, E. M. (2004), Relation between the global-warming parameter and the heat balance on the Earth's surface at increased contents of carbon dioxide, *Izvestiya, Atmos. Ocean. Phys.*, *40*, 269–275.

Webb, M., C. Senior, S. Bony, and J.-J. Morcrette (2001), Combining ERBE and ISCCP data to assess clouds in the Hadley Centre, ECMWF and LMD atmospheric climate models, *Climate Dyn.*, *17*, 905–922.

Wielicki, B. A., et al. (2002), Evidence for large decadal variability in the tropical mean radiative energy budget, *Science*, *295*, 841–844.

Wood, R., and C. S. Bretherton (2004), Boundary layer depth, entrainment, and decoupling in the cloud-capped subtropical and tropical marine boundary layer, *J. Climate*, *17*, 3576–3588.

Wyant, M. C., C. S. Bretherton, J. T. Bacmeister, J. T. Kiehl, I. M. Held, M. Z. Zhao, S. A. Klein, and B. J. Soden (2005), A comparison of tropical cloud properties and responses in GCMs using mid-tropospheric vertical velocity, *Climate Dyn.*, *Submitted*.

Yao, M.-S., and A. D. D. Genio (1999), Effects of cloud parameterization on the simulation of climate changes in the GISS GCM, *J. Climate*, *12*, 761–779.

Zhang, Y., W. B. Rossow, A. A. Lacis, V. Oinas, and M. I. Mishchenko (2004), Calculation of radiative fluxes from the surface to top of atmosphere based on ISCCP and other global data sets: Refinements of the radiative transfer model and the input data., *J. Geophys. Res.*, *109*, D19,105, doi:10.1029/2003JD004,457.

Sandrine Bony, Laboratoire de Météorologie Dynamique, IPSL, case courrier 99, 4 Place Jussieu, 75252 Paris cedex 05, France. (bony@lmd.jussieu.fr)

Received 24 June 2005; revised 30 August 2005; accepted 21 September 2005; published 26 October 2005.

Supporting Material

Marine Boundary Layer Clouds at the Heart of

Cloud Feedback Uncertainties in Climate Models

S. Bony and J.-L. Dufresne

LMD/IPSL, Paris, France

	∂C_ω^{SW}		∂C_ω^{LW}		∂C_ω^{NET}	
	ERA40	NCEP2	ERA40	NCEP2	ERA40	NCEP2
-60 hPa/d	0.77	0.87	0.81	0.82	0.53	0.69
-40 hPa/d	0.83	0.85	0.82	0.87	0.37	0.56
-20 hPa/d	0.80	0.81	0.87	0.75	0.43	0.59
0 hPa/d	0.81	0.81	0.93	0.88	0.52	0.54
20 hPa/d	0.80	0.85	0.85	0.89	0.72	0.77
30 hPa/d	0.87	0.87	0.80	0.85	0.84	0.86
40 hPa/d	0.94	0.93	0.83	0.88	0.92	0.91
50 hPa/d	0.93	0.97	0.73	0.89	0.91	0.96

Table 1: Correlation coefficient between the time series of the SW, LW and NET CRF interannual anomalies derived from ISCCP-FD and ERBE datasets over the period 1985-89. Correlations are reported for different dynamical regimes, defined either from ERA40 or NCEP2 reanalysis.

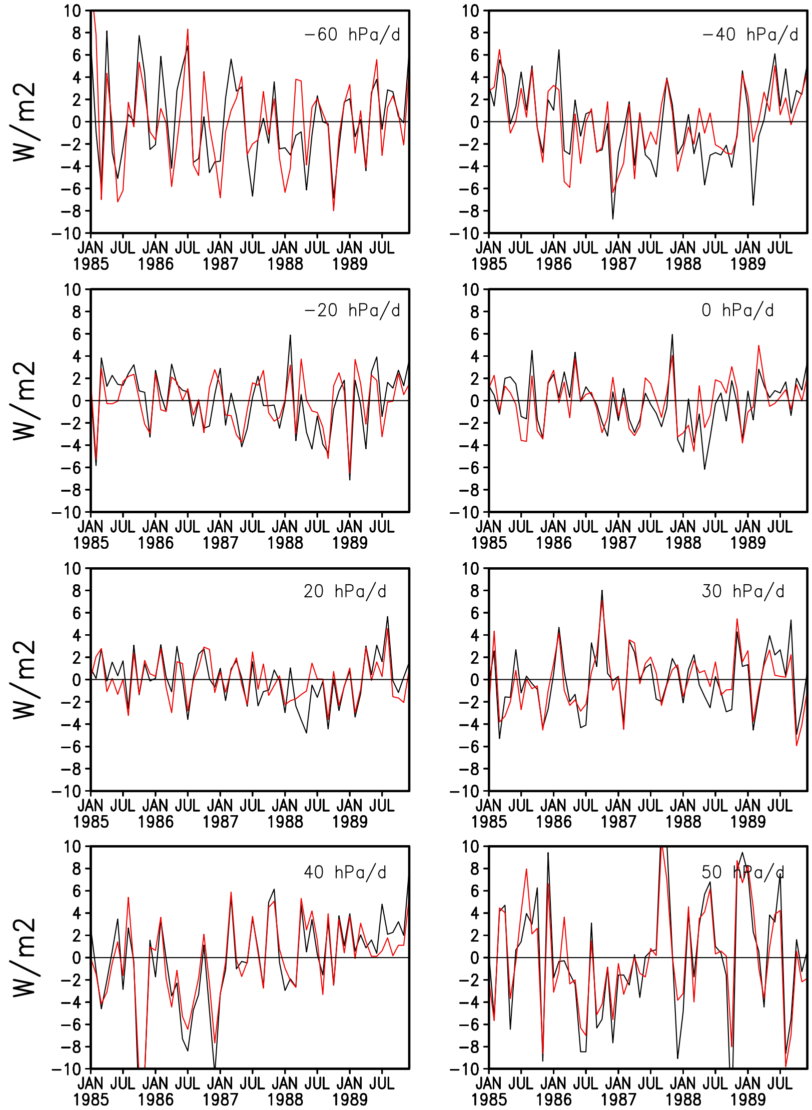

1

Figure 1: Interannual anomalies of the SW CRF derived from the ISCCP-FD dataset (in red) and from the Earth's Radiation Budget Experiment (ERBE, in black) over the period January 1985 - December 1989. The comparison is presented for different dynamical regimes defined from ERA40 500 hPa vertical pressure velocity.

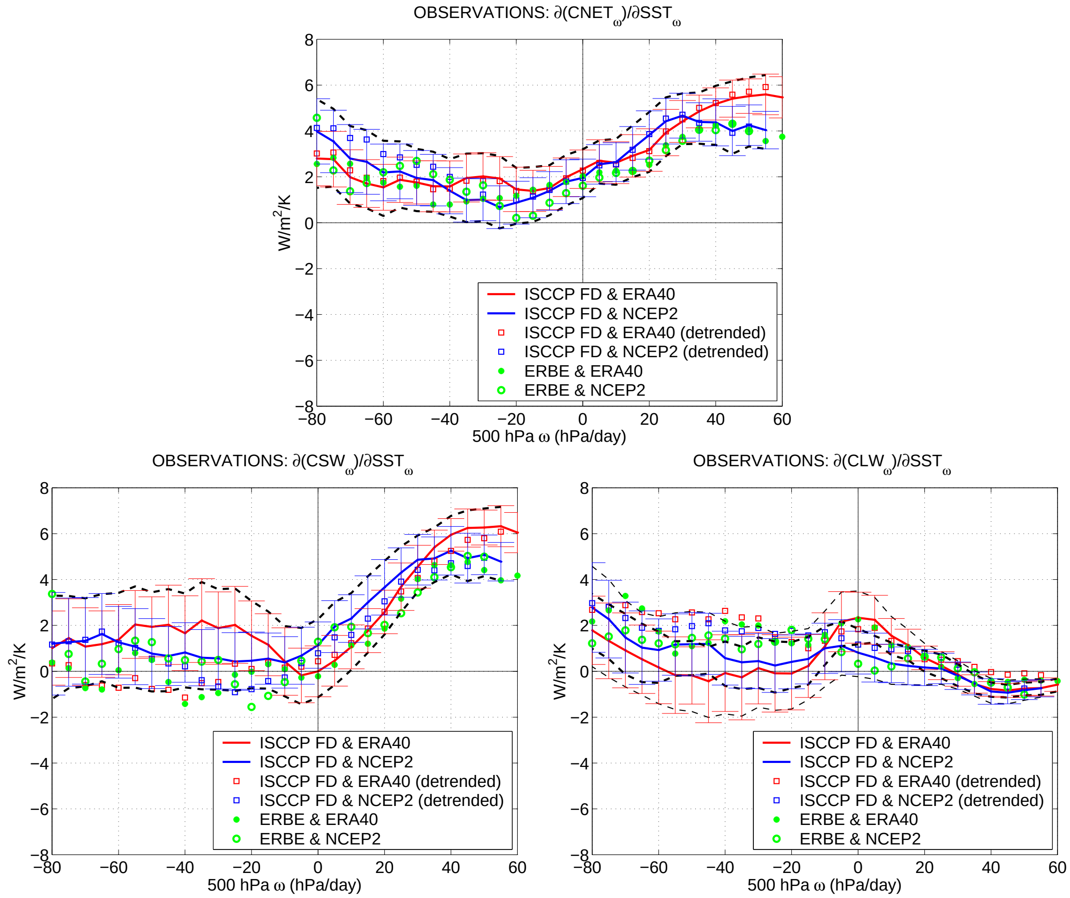

Figure 2: Observational estimates of the interannual sensitivity of the (top) NET, (middle) SW and (bottom) LW components of the CRF to SST: estimates are computed by using ISCCP-FD CRF data and meteorological reanalyses (either ERA40 or NCEP2) over the period 1984-2000. The sensitivity computed within each dynamical regime is associated with a 5%-95% confidence interval. The envelope of the ISCCP-FD/ERA40 and ISCCP-FD/NCEP2 confidence intervals defines the observational range of estimates used in our study. Also reported are the mean sensitivities computed from ERBE CRF data over a much shorter period (1985-89). ISCCP-FD radiation fluxes and ERA40 vertical velocities exhibit some decadal "trends" over the period 1984-2000. As shown by these figures, the sensitivities estimated from detrended data do not differ significantly from those estimated from raw data (particularly in subsidence regimes).

#	AOGCM	resolution	Σ (W/m^2/K)	ΔT (K)
1	CCSM3	256 x 128	-2.0	1.1
2	FGOALS-g1.0	128 x 60	-1.0	0.9
3	INM-CM3.0	72 x 45	-1.0	1.2
4	UKMO-HadCM3	96 x 73	-0.4	1.4
5	GFDL-CM2.0	144 x 90	-0.3	1.3
6	GISS-EH	72 x 46	-0.3	1.4
7	GISS-ER	72 x 46	-0.2	1.3
8	ECHAM5/MPI-OM	192 x 96	0.0	1.8
9	GFDL-CM2.1	144 x 90	0.1	1.3
10	UKMO-HadGEM1	192 x 145	0.1	1.5
11	CGCM3.1(T47)	96 x 48	0.9	1.7
12	CNRM-CM3	128 x 64	1.0	1.4
13	IPSL-CM4	96 x 72	1.0	1.6
14	MIROC3.2(medres)	128 x 64	1.5	1.8
15	MIROC3.2(hires)	320 x 160	1.6	2.3

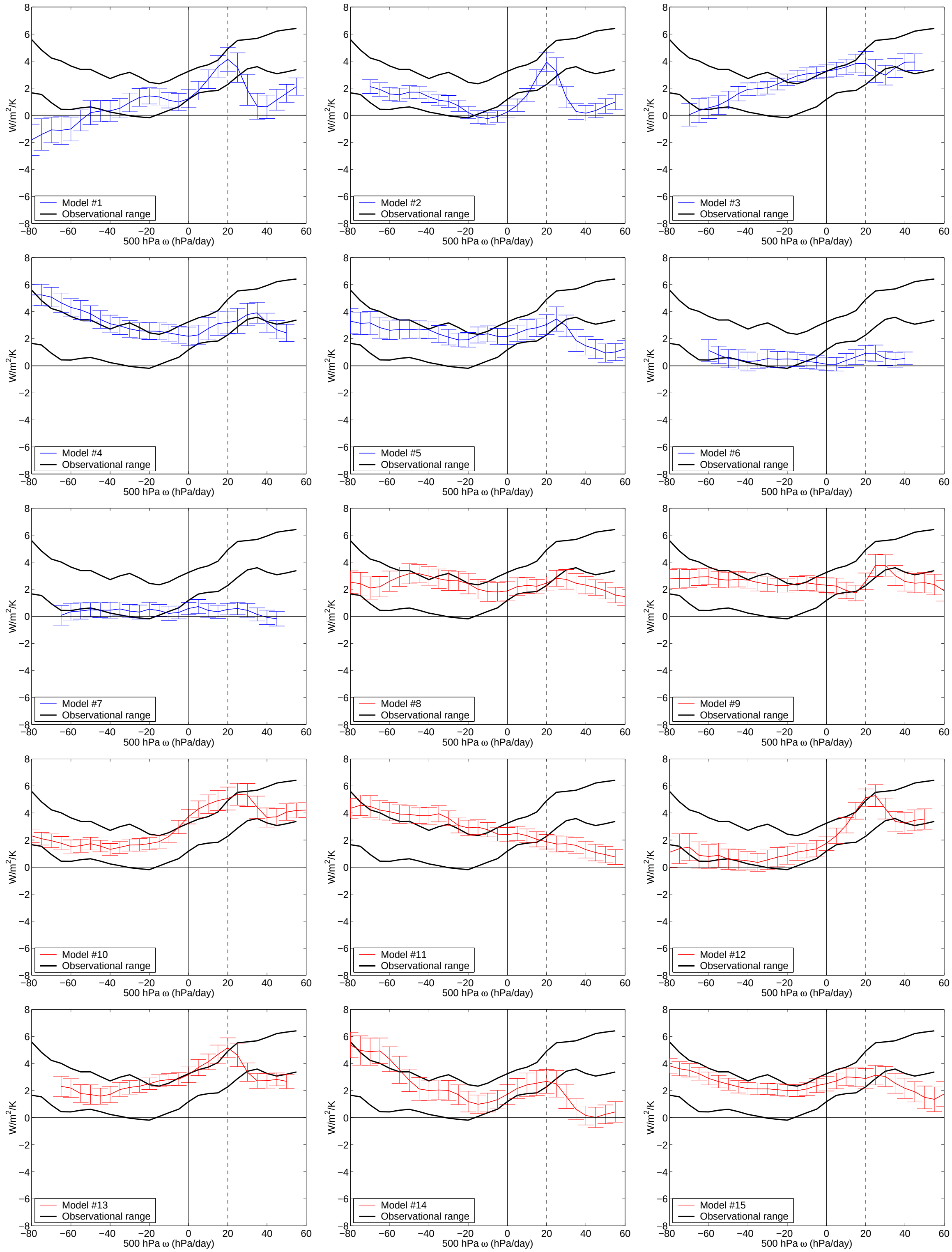

Figure 3: Comparison with observations of the interannual sensitivity of the NET CRF to SST (computed in dynamical regimes) derived from each coupled ocean-atmosphere general circulation model; models that predict $\Sigma < 0$ in climate change are in blue, models that predict $\Sigma > 0$ are in red.

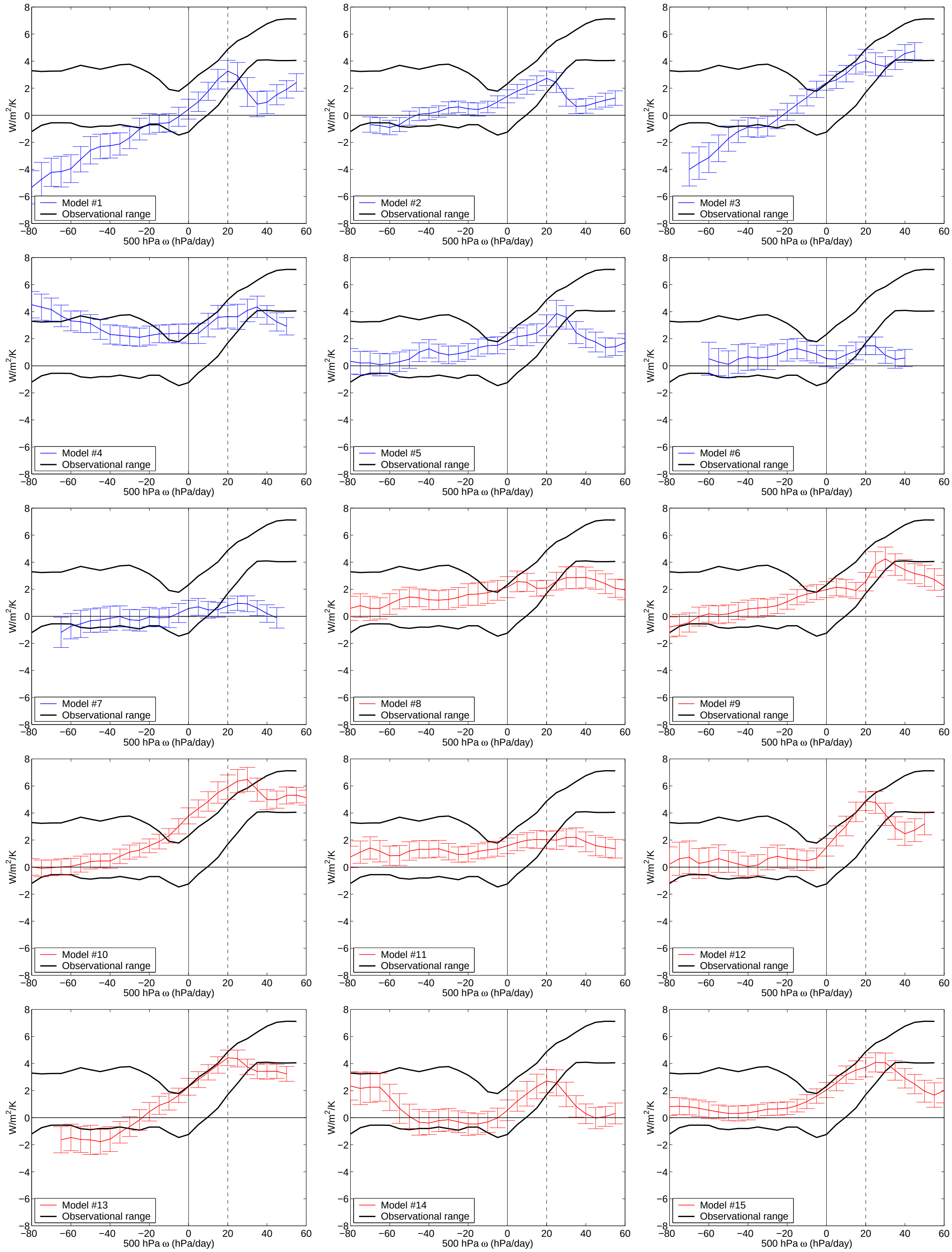

Figure 4: Comparison with observations of the interannual sensitivity of the SW CRF to SST (in dynamical regimes) derived from each coupled ocean-atmosphere general circulation model; models that predict $\Sigma < 0$ in climate change are in blue, models that predict $\Sigma > 0$ are in red.

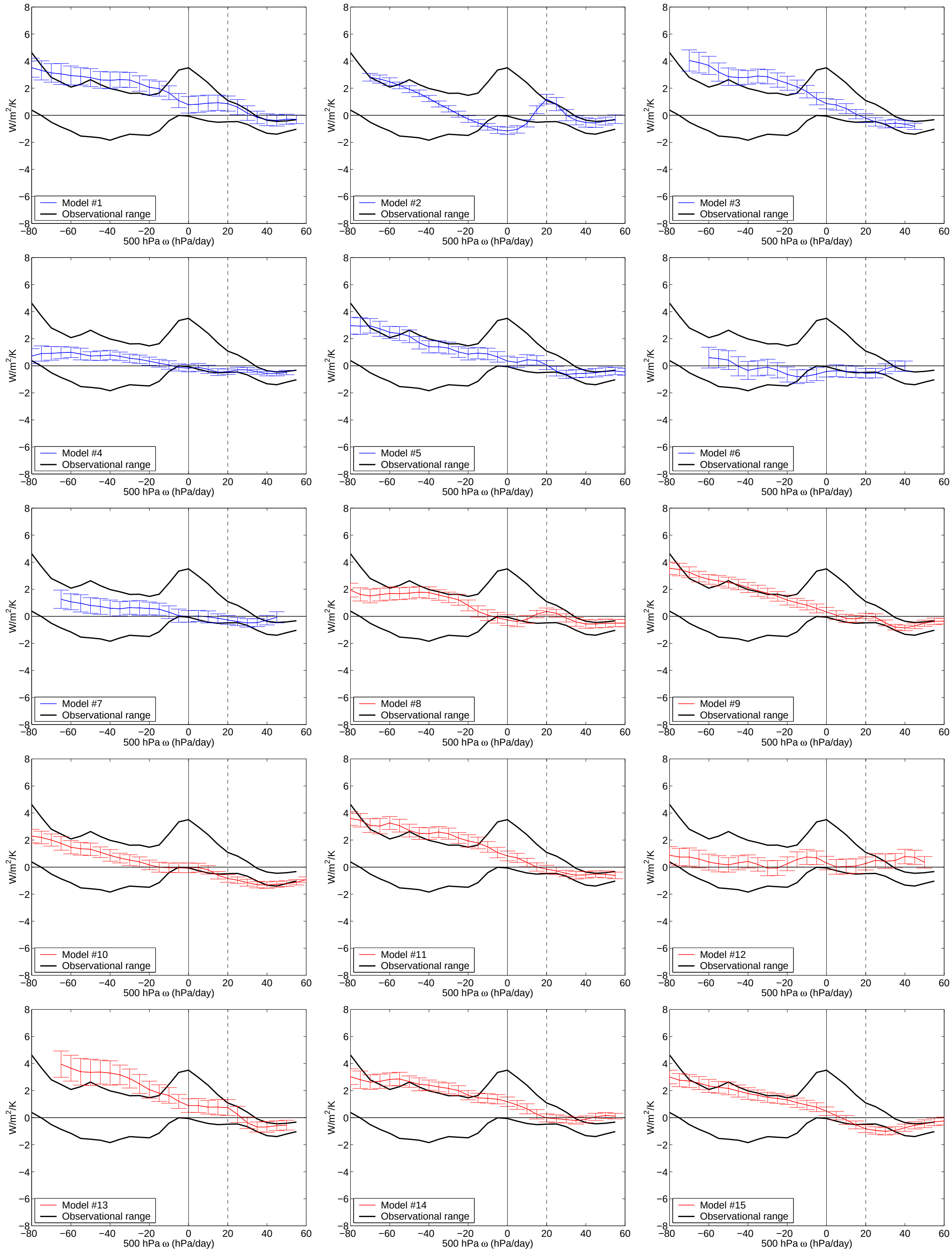

Figure 5: Comparison with observations of the interannual sensitivity of the LW CRF to SST (in dynamical regimes) derived from each coupled ocean-atmosphere general circulation model; models that predict $\Sigma < 0$ in climate change are in blue, models that predict $\Sigma > 0$ are in red.